PROCEEDINGS OF SPIE

SPIEDigitalLibrary.org/conference-proceedings-of-spie

Equivalent circuit modeling of traveling-wave superconducting-nanostripe single-photon detectors for silicon quantum photonic integrated circuits

Loïc Djamen Tchapda, Anindya Bal, Sami Nazib, Troy Hutchins-Delgado, Hosuk Lee, et al.

Loïc H. Djamen Tchapda, Anindya Bal, Sami A. Nazib, Troy A. Hutchins-Delgado, Hosuk Lee, Mark V. Reymatias, Erika M. Sommer, Ivan Komissarov, John Nogan, Tzu-Ming Lu, Roman Sobolewski, Marek Osiński, "Equivalent circuit modeling of traveling-wave superconducting-nanostripe single-photon detectors for silicon quantum photonic integrated circuits," Proc. SPIE 12415, Physics and Simulation of Optoelectronic Devices XXXI, 124150B (10 March 2023); doi: 10.1117/12.2654772

SPIE.

Event: SPIE OPTO, 2023, San Francisco, California, United States

Equivalent circuit modeling of traveling-wave superconducting-nanostripe single-photon detectors for silicon quantum photonic integrated circuits

Loïc H. Djamen Tchapda, Anindya Bal[1], Sami A. Nazib[1], Troy A. Hutchins-Delgado[1], Hosuk Lee[1], Mark V. Reymatias[1], Erika M. Sommer[1], Ivan Komissarov[2], John Nogan[3], Tzu-Ming Lu[3], Roman Sobolewski[2], and Marek Osiński[1]

[1]Center for High Technology Materials, University of New Mexico, 1313 Goddard St. SE, Albuquerque, NM 87106-4343, USA
[2]Department of Electrical and Computer Engineering, University of Rochester, NY 14627-0231, USA
[3]Center for Integrated Nanotechnologies, Sandia National Laboratories, 1000 Eubank SE, Albuquerque, New Mexico 87123, USA

ABSTRACT

Superconducting nanostripe single-photon detectors (SNSPDs) represent key components in silicon quantum photonic integrated circuits (SiQuPICs). They provide good timing precision, low dark counts, and high efficiency. The design, fabrication, and characterization of SiQuPICs comprising SNSPDs coupled to dielectric optical waveguides are the core objectives of our work. The detectors are positioned directly on the dielectric waveguide core to increase photon absorption by the superconducting nanostripes. We also present results on the SPICE circuit modeling of traveling-wave SNSPDs integrated with Si_3N_4/SiO_2 optical waveguides.

Keywords: Silicon quantum photonic integrated circuits, superconducting nanostripe single-photon detectors, SNSPDs, SPICE modeling, rise time, fall time.

1. INTRODUCTION

Traveling-wave superconducting nanostripe single-photon detectors (TW SNSPDs) integrated on Si substrates are expected to be the basic photon counting and sensing tools for future silicon quantum photonic integrated circuits (SiQuPICs). SNSPDs are currently the best detectors for counting and sensing photons over a wide range of wavelengths, from visible to mid-infrared range. They can achieve detection efficiencies close to 100%, which is essential for the successful implementation of high-performance quantum systems.

The most common SNSPD design consists of large-area (typically 10×10 μm2) square meanders, with photons approaching the device at the direction normal to the detector plane [Korneev 2017]. Such approach is not suitable for SiQuPICs, since the SNSPD sensing element, a superconducting nanostripe, must be in-plane with the incoming photon flux directed by a waveguide. This requires a different, non-meander geometry. For an SNSPD efficiently coupled to a dielectric optical waveguide, the best device geometry is a traveling-wave structure, described for the first time in [Kahl 2015] and more recently reviewed in [Ferrari 2018]. In our implementation, the superconducting nanostripe is deposited directly on top of an optical waveguide core and covered with the waveguide cladding, thus maximizing probability of the photon getting absorbed. If the interaction distance is long enough, the probability of a photon being absorbed will be close to unity.

SNSPDs have the specific benefit of high speed. Dark counts are mostly responsible for the noise in SNSPDs. It was determined that the vortices crossing the nanostripe cross section, which were caused by thermal fluctuations or the current-assisted unbinding of vortex-antivortex complexes, were the source of the intrinsic dark counts [Yamashita 2011]. The lowest dark count rate reported to date is 10^{-4} counts/s [Shibata 2015].

Physics and Simulation of Optoelectronic Devices XXXI, edited by Bernd Witzigmann, Marek Osiński, Yasuhiko Arakawa, Proc. of SPIE Vol. 12415, 124150B
© 2023 SPIE · 0277-786X · doi: 10.1117/12.2654772

In this paper, we focus on equivalent-circuit modeling of TW SNSPDs integrated with passive optical waveguides on a single Si chip.

2. SILICON QUANTUM PHOTONIC INTEGRATED CIRCUIT DESIGN

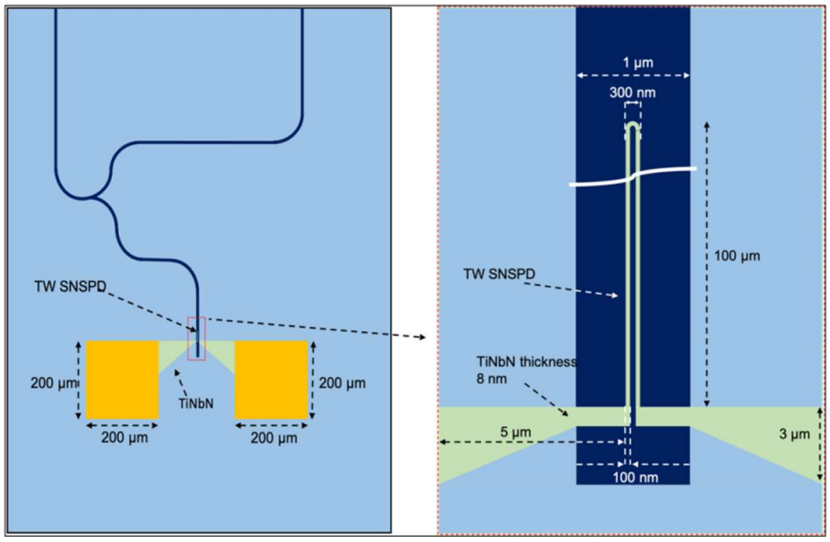

Fig. 1. Design of a SiQuPIC suitable for a direct integration with a quantum information circuit on a single silicon platform. The left panel shows the entire element together with input and reference optical waveguides, while the right panel (inset) presents a single-meander TW SNSPD in detail, placed directly on top of a dielectric waveguide core.

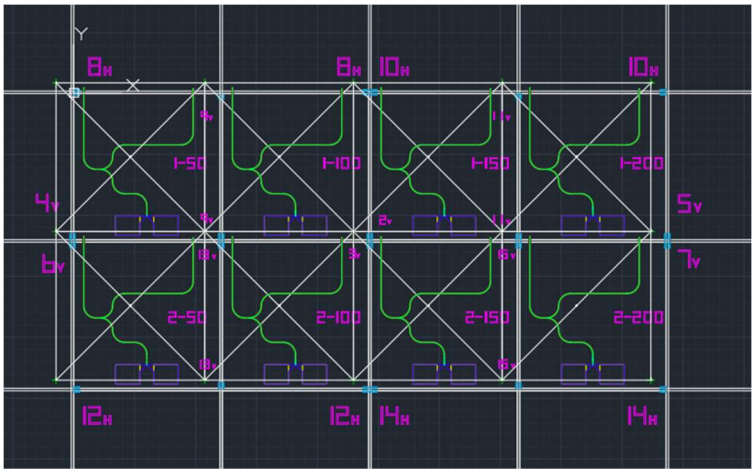

Fig. 2. Overview of the 8 devices designed for different meander numbers and segment lengths.

In our design, shown in Fig. 1, the SNSPDs are integrated with single-mode waveguides carrying externally injected photons. A single-mode optical fiber connected to the upper left waveguide allows for the introduction of single photons from an external source. A Y-junction splitter sends the photons either to a TiNbN TW SNSPD in the bottom portion of the chip, or to an external detector at the end of another single-mode fiber connected to the output waveguide. the dielectric waveguides consist of an 8-µm-thick SiO_2 layer placed on top of a Si substrate, a 1-µm-wide Si3N4 core with a core thickness ranging from 100 to 300 nm, and a 6-µm-thick top cladding of SiO_2. The ridge waveguide extends laterally by 2.5 µm on each side of the core. The Si_3N_4 waveguide core is in direct contact with a superconducting nanostripe that is centered on the waveguide axis in order to allow the stripe to absorb the evanescent field above the core. The guided mode

profile in the optical fiber must closely match the mode profile in the straight region of the narrow funnel-taper at the chip's edge [Zhu 2016] in order to enhance the coupling efficiency between the fiber transporting photons from an external source to the on-chip waveguide, as well as from the chip to the reference fiber.

Eight alternative designs of TW SNSPDs were considered. Fig. 2 shows a photolithography mask contour containing the eight versions of corresponding SiQuPICs. While details of the TW SNSPD designs cannot be seen on Fig. 2, they are identified by labels 1-50, 1-100, *etc*., until 2-200. The first digit indicates the number of meanders, while the second number corresponds to the length of single segments in each meander. The single segment lengths were 50 µm, 100 µm, 150 µm, and 200 µm, while the number of meanders varied from 1 to 2. The nanostripe width was fixed at w = 100 nm and the thickness was assumed to be d = 5 nm.

3. SPICE MODELING OF TRAVELING-WAVE SUPERCONDUCTING NANOSTRIPE SINGLE-PHOTON DETECTORS

By modeling the detector, we can account for the external characterizing circuit characteristics and optimize the device parameters for overall performance. The overall performance parameters include detection efficiency, output response power, output response recovery time, maximum counting rate, and timing jitter. The statistical absorption of the photon over the segment length l and the signal propagation delay along the nanostripe are the factors resulting in timing jitter [Tyler 2016]. Specifications for the readout circuit frequency responsiveness, readout line impedance, and trigger source type (voltage source) are all included in the external characterizing circuit. The detector output recovery time is impacted by readout line impedance, which may also result in latching. The nanostripe operates electrically as an inductor in the superconducting state, where the source of the inductance is mostly kinetic inductance rather than geometric inductance [Kerman 2007].

3.1. TW-SNSPD Modeling (SPICE Circuit Model 1)

The equivalent circuit of Fig. 3, suggested in [Berggren 2018], provides a foundation for the SPICE modeling of TW-SNSPDs. The four terminal elements (the gate, the gate return, the drain, and the source) allow us to simulate all major aspects of the device activity.

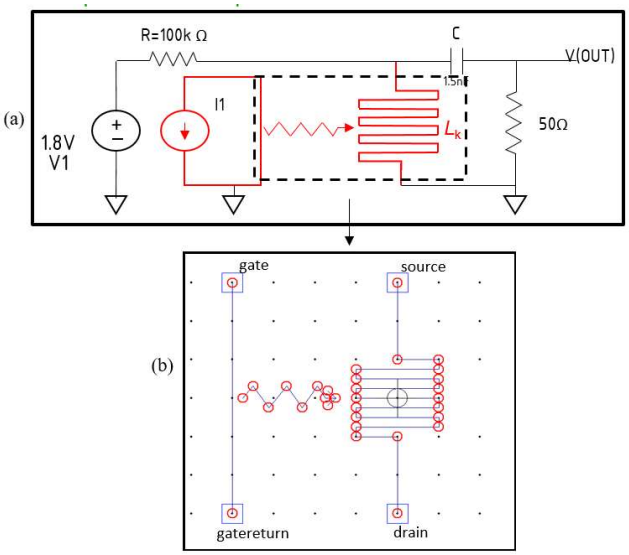

Fig. 3. (a) Simulation for single-photon incidence by 1-µA current with a 100-ps pulsewidth. (b) Single-photon detector within an equivalent circuit.

A method for introducing a photon-detection event is also needed in the equivalent circuit model. Short-lived hotspots caused by photon absorption lower the cross-sectional area across which the superconducting current may travel. We inserted a 100-ps current spike into the section of the nanostripe that the model utilized to detect the device state in order

to mimic this effect. While a photon arrival and absorption are simulated by the gate and gate-return terminals, current flow is simulated by the drain and source terminals, which are coupled to an external circuit. By modeling the detector, we may choose the best device settings while maximizing overall performance and taking into consideration the requirements of the external characterizing circuit. The total nanostripe length l_{tot} affects the detection efficiency. Timing jitter is produced by the statistical photon absorption process along the nanostripe length combined with the signal propagation delay. The trigger source type (voltage source), readout line impedance, and readout circuit frequency responsiveness are among the external readout circuit parameters. The readout line impedance might lead to latching if it is too large and has an impact on the detector output recovery time. The nanostripe operates electrically as an inductor in the superconducting state, where the source of the inductance is virtually completely kinetic rather than geometric.

3.2. TW-SNSPD Modeling (SPICE Circuit Model 2)

The source and drain are the terminals linked to an external readout circuit, while the gate and gate return terminals are utilized to simulate a photon arrival and absorption. Electrically, the superconducting nanostripe functions as an inductor with inductance L_k. Modeling the SNSPD as an inductor with a parametrically specified inductance involves describing the flux as $L_k I_{bias}$ in the inductor.

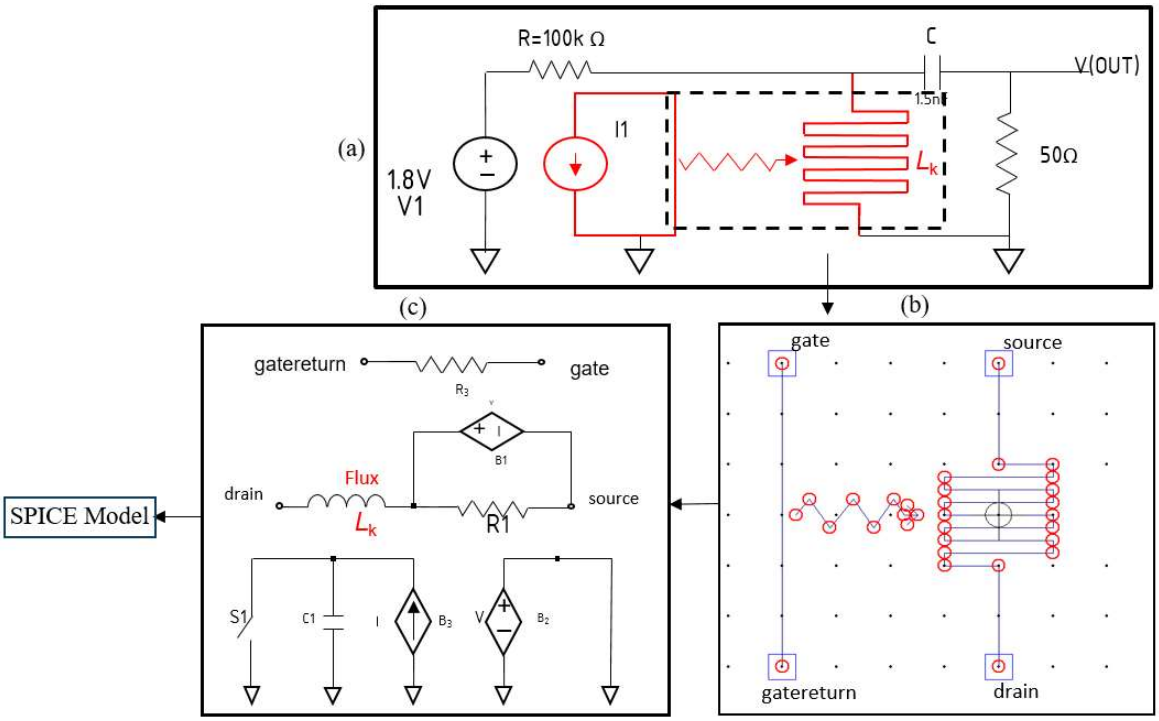

Fig. 4. (a) Circuit used to simulate single-photon absorption events by 1-μA amplitude, 100-ps width current pulses at 20 ns intervals; (b) SNSPD representation; (c) Dynamic circuit model.

We used the electrothermal model [Miki 2009] to simulate the hotspot development. In the range L = 6–605 nH and with load impedances of 20 Ω–1 kΩ and device switching currents of 20 μA, this model has been experimentally validated. Before depending on this model outside of this range, verification should be carried out. Yet the characteristics of a typical SNSPD device are included in this range.

4. SIMULATION PARAMETERS

In this section, we specify device parameters that were used in the simulations. The majority of the geometric and material properties needed for an accurate model of the device may be determined via electrical experiments.

4.1. Key Simulation Parameters

Symbol	Name of the Parameter	Values
l_{tot}	Overall nanostripe length(in μm)	$2l$ × # of meanders
w	Nanostripe width	100 nm
d	Nanostripe thickness	5 nm
ρ	NbTiN resistivity at 20 K	$122.5*10^{-8}$ Ω×m
I_{sh}	Switching current	20 μA
R_{sh}	Sheet resistance	ρ/d = 24.5 Ω/square
T_c	Critical temperature	10.5 K
T_{sub}	Substrate temperature	4.2 K
# of squares	Number of squares	l_{tot}/w
L'	Inductivity	27 pH/square
L	Inductance (in nH)	L' × # of squares

4.2. Individual Device Parameters

1-50 device	1-100 device	1-150 device	1-200 device
l_{tot} = 2 × 50 μm = 100 μm # of squares = 1000 L' = 27 pH/square L = 27 nH	l_{tot} = 2 × 100 μm = 200 μm # of squares = 2000 L' = 27 pH/square L = 54 nH	l_{tot} = 2 × 150 μm = 300 μm # of squares = 3000 L' = 27 pH/square L = 81 nH	l_{tot} = 2 × 200 μm = 400 μm # of squares = 4000 L' = 27 pH/square L = 108 nH
2-50 device	2-100 device	2-150 device	2-200 device
l_{tot} = 4 × 50 μm = 200 μm # of squares = 2000 L' = 27 pH/square L = 54 nH	l_{tot} = 4 × 100 μm = 400 μm # of squares = 4000 L' = 27 pH/square L = 108 nH	l_{tot} = 4 × 150 μm = 600 μm # of squares = 6000 L' = 27 pH/square L = 162 nH	l_{tot} = 4 × 200 μm = 800 μm # of squares = 8000 L' = 27 pH/square L = 216 nH

5. SIMULATION RESULTS

5.1. Output Voltage Response

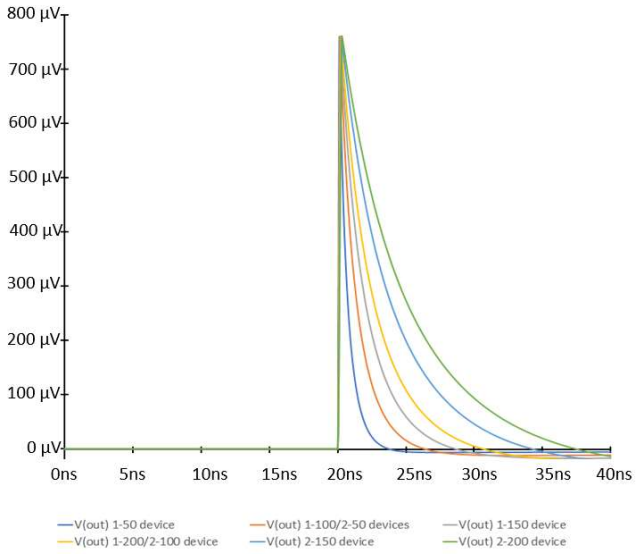

Fig. 5. Output voltage response over 20 ns for a 100-picosecond absorption pulse occurring at t = 20 ns (40 ns simulation range).

The computed output voltage response to a single-photon absorption event occurring at $t = 20$ ns is shown in Fig. 5 for all 6 cases of non-equivalent SNSPDs. The kinetic inductance of the detector determines the time to recovery, which rises with total detector length l_{tot}. The computed fall time is 1.42 ns for the smallest detectors ($l_{tot} = 100$ μm), rising to 10.04 ns for the largest detectors ($l_{tot} = 800$ μm).

Table 1.Rise times, fall times, and waveform widths for various SNSPD devices

	Inductances (L)	Rise times (10% to 90%)	Fall times (90% to 10%)	Waveform widths (50% to 50%)
1-50 Device	27 nH	0.07 ns	1.42 ns	0.46 ns
1-100 / 2-50 Devices	54 nH	0.10 ns	2.85 ns	0.90 ns
1-150 Device	81 nH	0.13 ns	4.20 ns	1.30 ns
1-200 / 2-100 Devices	108 nH	0.14 ns	5.43 ns	1.69 ns
2-150 Device	162 nH	0.17 ns	7.78 ns	2.48 ns
2-200 Device	216 nH	0.20 ns	10.04 ns	3.28 ns

5.2. Latching

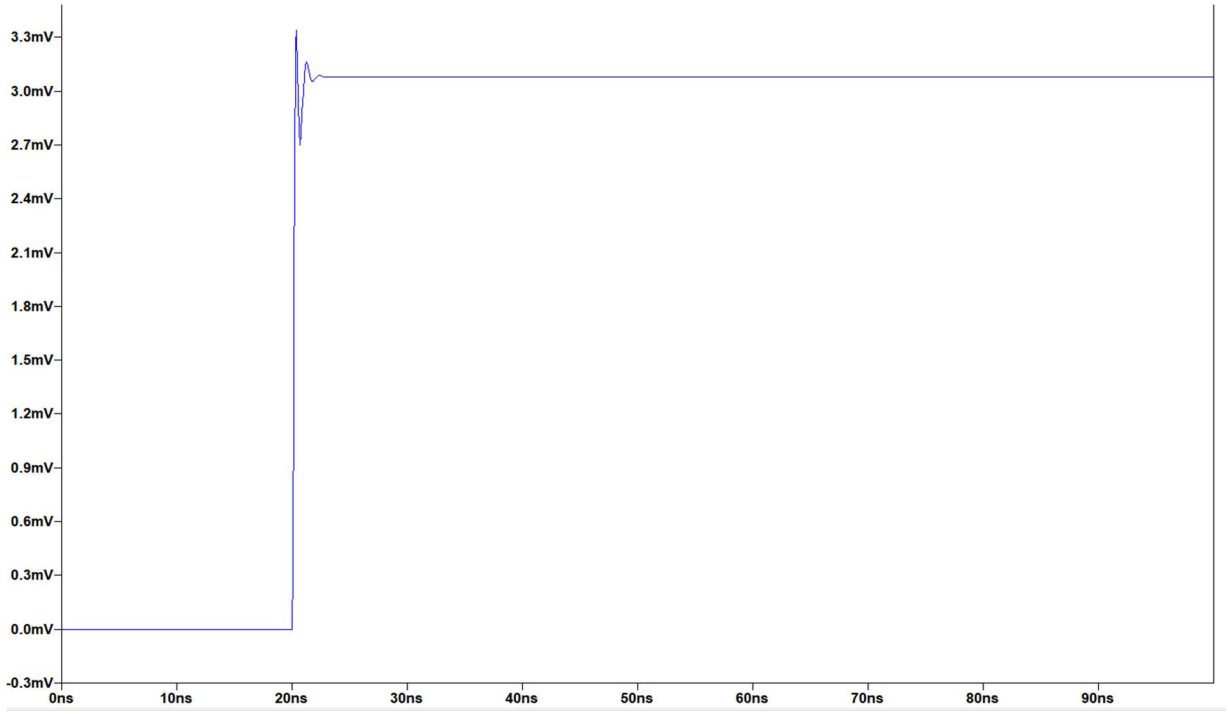

Fig. 6. Latching output voltage response over 80 ns for a 100-ps absorption pulse occurring at 20 ns intervals (100 ns simulation range).

When SNSPDs are coupled to a load and biased near to their critical current, the electrical regeneration of their current may occur so quickly that the current bias can be restored before the device has finished cooling. The device may then

revert to its initial phase and latch into a steady resistive state. The detector in this state is no longer sensitive to upcoming photon-arrival events. This action is referred to as latching [Annunziata 2010]. Using the entire dynamic model, the device was simulated to determine condition under which latching would occur. Fig. 6 shows an example of a latched response. As can be seen from Table 2, for all devices, readout line resistance that causes latching increases with l_{tot}. The maximum readout line resistance for the shortest detectors is 76 Ω, while it rises to 205 Ω for the longest ones.

Table 2. Readout line resistance causing latching for various SNSPD devices

	Inductances (L)	Max. Readout Line Resistances (R)
1-50 Device	27 nH	76 Ω
1-100 / 2-50 Devices	54 nH	102 Ω
1-150 Device	81 nH	125 Ω
1-200 / 2-100 Devices	108 nH	140 Ω
2-150 Device	162 nH	176 Ω
2-200 Device	216 nH	205 Ω

6. CONCLUSIONS

A SPICE model for TW SNSPDs has been created to facilitate the design of devices, with varying segment lengths and meander numbers. The 8 devices modeled were the single-meander TW SNSPDs with single-segment length of 50 μm, 100 μm, 150 μm, and 200 μm, and double-meander TW SNSPDs with single-segment lengths of 50 μm, 100 μm, 150 μm, and 200 μm. Simulations show that the maximum counting rate decreases with the overall nanostripe length l_{tot}, while the output signal power increases with l_{tot}. Our findings support the notion that the waveguide-coupled TW SNSPD is a highly promising detector design for SiQuPICs and is particularly well suited for demonstrations of cryogenic quantum information processing.

7. ACKNOWLEDGEMENTS

The authors acknowledge financial support from the National Science Foundation under the grants ECCS-1842712 “RAISE-EQuIP: Integrated Silicon Photonics Platforms for Scalable Quantum Systems” and OIA-2217786 “RII Track-2 FEC: Laying the Foundation for Scalable Quantum Photonic Technologies”. This work was performed, in part, at the Center for Integrated Nanotechnologies, an Office of Science User Facility operated for the U.S. Department of Energy (DOE) Office of Science by Los Alamos National Laboratory (Contract DE-AC52-06NA25396) and Sandia National Laboratories (Contract DE-NA-0003525), under the User Project #2019BU0169.

8. REFERENCES

[Annunziata 2010] A. J. Annunziata, O. Quaranta, D. F. Santavicca, A. Casaburi, L. Frunzio, M. Ejrnaes, M. J. Rooks, R. Cristiano, S. Pagano, A. Frydman, and D. E. Prober, “Reset dynamics and latching in niobium superconducting nanowire single-photon detectors”, *J. Appl. Phys*. **108** (#8), Art. 084507, 2010.

[Berggren 2018] K. K. Berggren, Q.-Y. Zhao, N. Abebe, M. J. Chen, P. Ravindran, A. McCaughan, and J. C. Bardin, “A superconducting nanowire can be modeled by using SPICE”, *Superconductor Science and Technology* **31** (#5), Art. 055010 (13 pp.), Apr. 2018.

[Ferrari 2018] S. Ferrari, C. Schuck, and W. Pernice, “Waveguide-integrated superconducting nanowire single-photon detectors”, *Nanophotonics* **7** (#11), pp. 1725-1758, 2018.

[Kahl 2015] O. Kahl, S. Ferrari, V. Kovalyuk, G. N. Goltsman, A. Korneev. and W. H. P. Pernice, “Waveguide integrated superconducting single-photon detectors with high internal quantum efficiency at telecom wavelengths”, *Scientific Reports* **5**, Art.10941 (4 pp.), 2015.

[Kerman 2007] A. J. Kerman, E. A. Dauler, J. K. Yang, K. M. Rosfjord, V. Anant, K. K. Berggren, G. N. Gol'tsman, and B. M. Voronov, “Constriction-limited detection efficiency of superconducting nanowire single-photon detectors”, *Appl. Phys. Lett*. **90** (#10), Art. 101110, 2007.

[Korneev 2017] A. Korneev, A. Semenov, D. Vodolazov, G. N. Gol'tsman, and R. Sobolewski, “Physics and Operation of Superconducting Single-Photon Devices”, in *Superconductors at the Nanoscale: From Basic Research to Applications* (R. Wördenweber and J. Vanacken, Eds.), Ch. 9, pp. 279-308 (De Gruyter Press, 2017), and references therein.

[Miki 2009] S. Miki, M. Takeda, M. Fujiwara, M. Sasaki, A. Otomo, and Z. Wang, “Superconducting NbTiN nanowire single photon detectors with low kinetic inductance”, *Appl. Phys. Express* **2** (#7), Art. 075002 (2009).

[Shibata 2015] H. Shibata, K. Shimizu, H. Takesue, and Y. Tokura, “Ultimate low system dark-count rate for superconducting nanowire single-photon detector”, *Opt. Lett.* **40**, pp. 3428-3431, 15 July 2015.

[Tyler 2016] N. A. Tyler, J. Barreto, G. E. Villarreal-Garcia, D. Bonneau, D. Sahin, J. L. O’Brien, and M. G. Thompson, "Modelling superconducting nanowire single photon detectors in a waveguide cavity“, *Opt. Express* **24**, pp. 8797-8808, 2016.

[Yamashita 2011] T. Yamashita, S. Miki, K. Makise, W. Qiu, H. Terai, M. Fujiwara, M. Sasaki, and Z. Wang, “Origin of intrinsic dark count in superconducting nanowire single-photon detectors”, *Appl. Phys. Lett.* **99** (#16), Art. 161105 (3 pp.), 2011.

[Zhu 2016] T. C. Zhu, Y. W. Hu, P. Gatkine, S. Veilleux, J. Bland-Hawthorn, and M. Dagenais, “Ultrabroadband high coupling efficiency fiber-to-waveguide coupler using Si_3N_4/SiO_2 waveguides on silicon”, *IEEE Photon. J*. **8** (#5), Art. 7102112 (12 pp.), Oct. 2016.